

Three-dimensional bond-order formation in kagome metals AV_3Sb_5 (A=Cs, Rb, K) analyzed by the density-wave equation method

Seiichiro Onari¹, Rina Tazai², Youichi Yamakawa¹, and Hiroshi Kontani¹

¹*Department of Physics, Nagoya University, Nagoya 464-8602, Japan*

²*Yukawa Institute for Theoretical Physics, Kyoto University, Kyoto 606-8502, Japan*

(Dated: August 22, 2024)

The mechanism of CDW and its 3D structure are important fundamental issues in kagome metals. We have previously shown that, based on a 2D model, 2×2 bond order (BO) emerges due to the paramagnon-interference (PMI) mechanism and that its fluctuations lead to *s*-wave superconductivity. This paper studies these issues based on realistic 3D models for kagome metals AV_3Sb_5 (A=Cs, Rb, K). We reveal that a commensurate 3D $2 \times 2 \times 2$ BO is caused by the PMI mechanism, by performing the 3D density-wave (DW) equation analysis for all A=Cs, Rb, K models in detail. Our results indicate a BO transition temperature $T_{BO} \sim 100K$ within the regime of moderate electron correlation. The 3D structure of BO is attributed to the three-dimensionality of the Fermi surface, while the 3D structure of BO is sensitively changed since the Fermi surface is quasi-2D. In the DW equation analysis, the most favorable 3D structure is (i) the alternating vertical stacking BO, where star-of-David (SoD) and tri-hexagonal (TrH) patterns stack alternatively. Other candidate is (ii) the shift-stacking BO composed of either SoD or TrH pattern. We find that the 3D structure of BO can be determined by the 3rd-order Ginzburg-Landau free energy $b\phi_1\phi_2\phi_3$. Since b depends sensitively on the band structure, both (i) and (ii) can be realized. The present study enhances our understanding of the rich variety of BOs observed experimentally. It is confirmed that the PMI mechanism is the essential origin of the 3D CDW of kagome metals.

I. INTRODUCTION

The multistage rich quantum phase transitions in the kagome-lattice superconductors AV_3Sb_5 (A=Cs, Rb, K) attract great attention in the field of condensed matter physics [1–3]. In each V-Sb plane, the 2×2 star-of-David (SoD) or tri-hexagonal (TrH) density wave (DW) is formed at $T_{BO} \approx 90$ K at ambient pressure [4, 5]. It is presumably the triple- \mathbf{q} (3Q) bond order (BO), which is the even-parity modulation in the hopping integral δt_{ij}^b (=real) [6–13]. Below T_{BO} , superconductivity (SC) appears at $T_{SC} \approx 1 \sim 3$ K, and it increases to 8 K under $P \approx 3$ GPa. At ambient pressure for A=Cs, the highly anisotropic *s*-wave SC state is realized [14, 15], which is naturally understood based on the BO fluctuation mechanism [12].

In a single V-Sb plane, the order parameters of the 3Q BO are expressed as $\phi = (\phi_1, \phi_2, \phi_3)$, where ϕ_m is the strength of the m th BO at wavevector \mathbf{q}_m ($m = 1, 2, 3$) as shown in Fig. 1 (a). In this paper, the thick purple bond (i, j) in a BO state is defined as $|t_{i,j} + \delta t_{i,j}| > |t_{i,j}|$, where $t_{i,j}$ and $\delta t_{i,j}$ are the hopping integral without BOs and the modulation in it, respectively. When $|\phi_m|$ is independent of m , ϕ corresponds to the SoD (TrH) for $\phi_1\phi_2\phi_3 > 0$ (< 0), as shown in Fig. 1 (b) (1 (c)). Each 3Q order is composed of 4 unit cells of kagome lattice, that is, 12 V atoms.

It is important to understand the BO state because it is an essential electronic property in kagome metals. Many theoretical researches have been performed. The BO is formed in the presence of strong off-site interaction I . Large I is mediated by the effective off-site electron correlations [6, 7, 9, 10, 12]. The bond-stretching phonon also mediates I [16]. The absence of acoustic

phonon anomaly at T_{BO} [17] indicates the important contribution from the electron correlations. In Ref. [12], the authors found that the BO is naturally induced by the “paramagnon-interference (PMI) mechanism”, which is dropped in the mean-field-type approximations. This mechanism naturally explains the orbital and bond orders observed in Fe-based and cuprates superconductors [18].

Recently, the three-dimensional (3D) nature of the BO in kagome metals has attracted increasing attention because it drastically changes the electronic properties of kagome metals. Depending on the carrier doping and the pressure, the BO states with period-1, period-2, and period-4 along the *c*-axis, which are called the $2 \times 2 \times C$ BO ($C = 1, 2, 4$), have been reported. In the case of $C = 2$, the SoD or TrH stacking is realized for $\{q_1^z, q_2^z, q_3^z\} = \{\pi, \pi, 0\}$, while SoD-TrH alternating stacking is realized for $\{q_1^z, q_2^z, q_3^z\} = \{\pi, 0, 0\}, \{\pi, \pi, \pi\}$, where q_m^z is the *z* component of wavevector in the m th BO.

In addition, the time-reversal-symmetry-breaking TRSB state has been observed by various experimental methods [4, 19–26]. As for the origin of the TRSB state, the chiral charge current order, which is the pure imaginary BO δt_{ij}^c (=imaginary), has been proposed [9–11, 13, 27, 28]. This topic attracts significant attention in kagome metals. The recent theoretical study [13] has revealed that the current order structure is strongly coupled to the background BO. Thus, the 3D nature of the BO is very important to understand the nematicity as well as the chiral current order.

In this paper, we study the 3D nature of the DW in kagome metals based on the realistic 3D multiorbital models for AV_3Sb_5 (A=Cs, Rb, K), by using the 3D DW equation method [12, 29–31]. The DW equation corre-

sponds to the 2nd-order Ginzburg-Landau (GL) free energy, which controls the transition temperature of the DW. We reveal that commensurate $2 \times 2 \times 2$ BO is realized by the PMI mechanism described by the Aslamazov-Larkin vertex corrections (AL-VCS) in all A=Cs, Rb, K models. The 3D structure of BO originates from that of the Fermi surface. In the DW equation analysis, the most favorable 3D structure is (i) the alternating vertical stacking BO (v-BO), where the star-of-David (SoD) and Tri-hexagonal (TrH) shape BOs stack alternatively. Other candidate (ii) the SoD or TrH shift-stacking BO (s-BO) is also energetically favorable in the PMI mechanism. Both s-BO states can be realized by considering the 3rd-order GL free energy $b\phi_1\phi_2\phi_3$. These results are robust for all A=Cs, Rb, K models. The present study enhances our understanding of the rich variety of BOs observed experimentally. It is confirmed that the PMI mechanism is the essential origin of the 3D CDW of kagome metals.

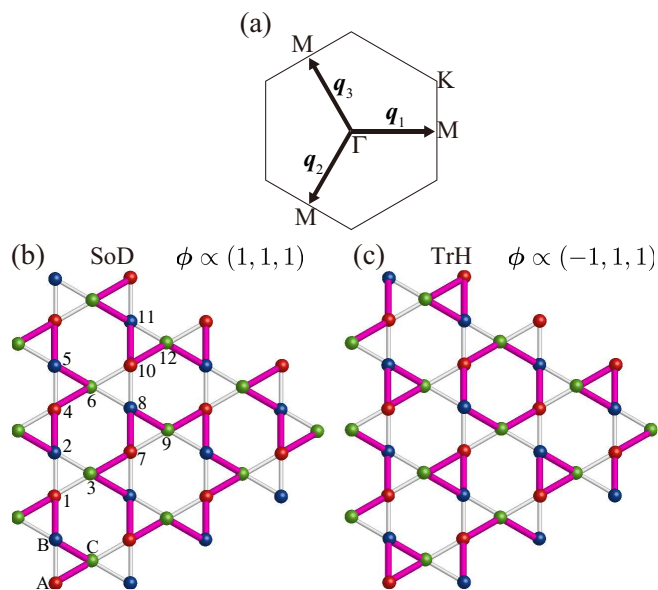


FIG. 1. (a) 2D wavevector \mathbf{q}_m ($m = 1, 2, 3$) in the original 2D Brillouin zone. (b) 2D SoD BO that corresponds to $\phi \propto (1, 1, 1)$. In the BO state, the thick purple bond (i, j) is defined as $|t_{i,j} + \delta t_{i,j}| > |t_{i,j}|$ in this paper. (c) 2D TrH BO that corresponds to $\phi \propto (-1, 1, 1)$.

Here, we present a brief summary of the CDW structure observed in AV_3Sb_5 . In each layer, the 2×2 superlattice structure that indicates the formation of the 3Q CDW has been observed for A=Cs, Rb, and K [32–40]. Recently, the $2 \times 2 \times 1$ superlattice [41], the $2 \times 2 \times 2$ superlattice [41–53], and the $2 \times 2 \times 4$ superlattices [41, 51–55] have been observed in the CDW phase. In this study, we take account of the $2 \times 2 \times 1$ and $2 \times 2 \times 2$ CDW states for simplicity.

In the $2 \times 2 \times 2$ CDW state, (i) the alternating v-BO has been proposed by combining the ARPES measurement and the DFT first principles calculation in A=Cs [49].

On the other hand, (ii) the nematic SoD or TrH s-BO has been supported by the STM [42] the NMR [43–46], the ARPES [47, 49], and the X-ray [48, 50, 51] measurements for A=Cs, Rb, and K. In general, it is difficult to distinguish between the SoD and TrH BOs in experiments such as STM and X-ray measurements since the observed results can be interpreted by both the SoD and TrH BOs. Recently, the NMR/NQR studies at low temperatures [37, 56], which is suitable for observing local symmetry, have proposed the SoD BO. However, consensus of the BO states has yet to be reached in kagome metals since the observed BO depends on the doping, and pressure, and experimental method.

Theoretically, the TrH stacking CDW due to the electron-phonon interaction mechanism is obtained by the DFT first principles studies [57–60]. However, the change in the bond length obtained by the first principles studies is rather large compared to the experimental results [41, 51, 54]. Thus, it is reasonable to assume that the origin of the CDW is the electron correlation. As for the electron correlation mechanism, the 3D CDW formation due to the on-site and off-site Coulomb interaction has been studied based on the mean-field theory [61, 62] and the variational method [63], by introducing sizable off-site interactions.

In contrast, the present authors studied the realistic 2D kagome metal model based on the DW equation method by considering only the on-site Coulomb interaction U [12]. In the PMI mechanism, the effective off-site interaction is induced by the AL terms, which are the higher-order electron correlation. We revealed that the commensurate 2×2 CDW is naturally and robustly given by the PMI mechanism. In addition, *s*-wave superconductivity is explained by the CDW fluctuations. In this paper, we show that the same mechanism can explain the 3D CDW based on realistic 3D kagome metal models.

GL theories in 2D kagome metals have revealed that the 3Q 2×2 TrH or SoD CDW state is stabilized by the 3rd-order GL terms [10, 13, 62]. The coexistence of the 3Q CDW and chiral charge current orders is also expected by the GL theories. In the coexisting state, C_2 nematicity appears [13, 62].

The 3D structure of CDW has been discussed in Refs. [10, 64, 65] by using the 3D GL theory. The $2 \times 2 \times 2$ s-BO has been proposed by the 3D GL theory. In CsV_3Sb_5 , the TrH s-BO was proposed [64, 65], where the coefficients of the GL terms are estimated by the first principles calculation.

II. GINZBURG-LANDAU FREE ENERGY

Here, we discuss the 3D BO transition based on the GL theory. Hereafter, we denote a 3D variable wavevector $\mathbf{Q} = (\mathbf{q}, q^z)$, where \mathbf{q} (q^z) is the 2D (1D) variable wavevector. We also introduce the notation $\mathbf{Q}_m = (\mathbf{q}_m, q_m^z)$ ($m = 1, 2, 3$), where \mathbf{q}_m is the fixed 2D wavevector introduced in Fig. 1 (a), while q_m^z is treated as a

variable. In this study, we take account of commensurate $q_m^z = -q_m^z (= 0, \pi)$ BO wavevectors, which correspond to $2 \times 2 \times 1$ and $2 \times 2 \times 2$ BO.

We introduce the “form factor” of the BO at wavevector \mathbf{Q} , $\hat{g}_{\mathbf{Q}}(k)$, which is given by the Fourier transformation of the 3D BO, such as the 3D stacking of Figs. 1 (b) and (c). $k \equiv (\mathbf{k}, \epsilon_n)$, $\epsilon_n = (2n + 1)\pi T$ is the fermion Matsubara frequency. The form factor is normalized by setting $\max|\hat{g}_{\mathbf{Q}}(k)| = 1$. Here, $\hat{g}_{\mathbf{Q}}(k)$ is a 3×3 matrix with respect to the three sublattices A, B, and C. In this study, we derive the BO form factor and its eigenvalue $\lambda_{\mathbf{Q}}$ in 3D momentum space microscopically, by analyzing the DW equation for the 3D kagome metal models. It is found that both $\hat{g}_{\mathbf{Q}_m}(k)$ and $\lambda_{\mathbf{Q}_m}$ ($m = 1, 2, 3$) have very small q_m^z -dependences. By introducing the order parameters $\phi = (\phi_1, \phi_2, \phi_3)$, the potential of the BO state at $\mathbf{Q} = \mathbf{Q}_m$ is given as $\phi_m \hat{g}_{\mathbf{Q}_m}(k)$.

The GL free energy up to the 3rd-order term is

$$F = F^{(2)} + F^{(3)}, \quad (1)$$

$$F^{(2)} = \sum_{m=1}^3 a_m(q_m^z) \phi_m^2, \quad (2)$$

$$a_m(q_m^z) = \left(-1 + \frac{1}{\lambda_{\mathbf{Q}_m}} \right) \chi_g^0(\mathbf{Q}_m), \quad (3)$$

$$F^{(3)} = b_1(q_1^z, q_2^z, q_3^z) \phi_1 \phi_2 \phi_3, \quad (4)$$

where $\chi_g^0(q) = -\frac{T}{N} \sum_{k,l,l',m,m'} g_q^{ml}(k+q) G_{ll'}(k+q) G_{m'm}(k) g_q^{l'm'}(k)$ is the BO irreducible susceptibility given by the Green function \hat{G} and the BO form factor \hat{g} [13, 66]. We use \mathbf{k} meshes $N = N_x \times N_y \times N_z = 60 \times 60 \times 32$, and Matsubara frequency $N_\omega = 512$. Hereafter, the unit of the energy is eV unless otherwise noted. Based on the GL free energy, we consider the possible $2 \times 2 \times 2$ BO given by $\{q_1^z, q_2^z, q_3^z\} = \{\pi, \pi, 0\}$, $\{\pi, 0, 0\}$, $\{\pi, \pi, \pi\}$ or $\{0, 0, 0\}$. (Exactly speaking, $\{q_1^z, q_2^z, q_3^z\} = \{0, 0, 0\}$ is the $2 \times 2 \times 1$ BO.) First, we consider only the 2nd-order GL term. When $a_m(q_m^z)$ is independent of q_m^z , all $2 \times 2 \times 2$ BO states can be realized. When $a_m(0) < a_m(\pi)$, the $2 \times 2 \times 1$ BO with $\{q_1^z, q_2^z, q_3^z\} = \{0, 0, 0\}$ is realized. In contrast, when $a_m(0) > a_m(\pi)$, the $2 \times 2 \times 2$ BO with $\{q_1^z, q_2^z, q_3^z\} = \{\pi, \pi, \pi\}$, which is the “alternating v-BO” with C_6 symmetry shown in Fig. 2 (a), is the most favorable. Also, the $2 \times 2 \times 2$ BO with $\{q_1^z, q_2^z, q_3^z\} = \{\pi, \pi, 0\}$, which is the “SoD (TrH) s-BO” with nematic C_2 symmetry shown in Fig. 2 (b), is favored. The nematic director corresponds to the shift vector between the upper and lower layers. When $b_1 < 0$ ($b_1 > 0$), the SoD (TrH) BO in our definition will be realized.

Next, we consider the effect of the 3rd-order GL term when $a_m(q_m^z)$ is independent of q_m^z . Because the GL free energy is uniform, $b_1(q_1^z, q_2^z, q_3^z)$ can be finite only when $q_1^z + q_2^z + q_3^z = 0$ (modulo reciprocal lattice vector). Therefore, the 3rd-order GL term favors the SoD (TrH) s-BO with $\{q_1^z, q_2^z, q_3^z\} = \{\pi, \pi, 0\}$.

Therefore, various $2 \times 2 \times 2$ BO states can be realized within the GL free energy argument, depending on the q^z -dependences of $a_m(q^z)$ and $b_1(q_1^z, q_2^z, -q_1^z - q_2^z)$. In

later sections, we perform the numerical study of these coefficients based on the 3D multiorbital kagome metal models.

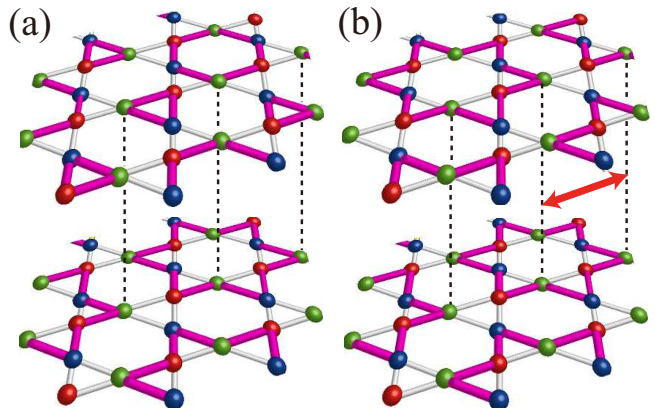


FIG. 2. Possible $2 \times 2 \times 2$ 3D BO states: (a) “alternating v-BO” with C_6 symmetry. (b) “SoD s-BO” with nematic C_2 symmetry. The red arrow represents the nematic director.

III. 3D MULTIORBITAL MODEL FOR KAGOME METAL

Here, we derive the first-principles realistic tight-binding model for CsV_3Sb_5 , by using the WIEN2k [67] and Wannier90 [68] software. The derived kinetic term is

$$H_0 = \sum_{\mathbf{k}, l, m, \sigma} c_{\mathbf{k}l\sigma}^\dagger h_{lm}^0(\mathbf{k}) c_{\mathbf{k}m\sigma}, \quad (5)$$

where \mathbf{k} is the 3D wavevector, l, m represents the d and p -orbitals, and σ is the spin index. To improve the tight-binding model, we introduce the energy shift of all Sb p -orbitals $\Delta E_p = -0.2$. The bandstructure of compared to that $\Delta E_p = 0$ is shown in Fig. 10 (a) in Appendix A. Energy at the Γ point $E_\Gamma \sim -0.4$ given for original $\Delta E_p = 0$ is reduced to $E_\Gamma \sim -0.55$ by introducing $\Delta E_p = -0.2$. Since $E_\Gamma \sim -0.55$ well reproduces the ARPES measurements [49, 69], $\Delta E_p = -0.2$ is reasonable for the model of CsV_3Sb_5 .

The 3D FS structure is shown in Fig. 10 (b) in Appendix A. The FSs at $n = 31$ (=original electron filling) are shown in Figs. 3 (a)-(c). Also, the FSs at $n = 30.8$ (=20% hole doping) are shown in Figs. 3 (d)-(f). These FSs are quasi-2D. The FSs in $k_z = 0$ are different between $n = 31$ and $n = 30.8$ due to the Lifshitz transition around the M point, while the FSs in $k_z = \pi$ at $n = 31$ are almost the same as those at $n = 30.8$. The FSs of A=Rb, K for $E_p = -0.2$ are shown in Fig. 4. The FSs of A=Rb, K are similar to those of the hole-doped A=Cs in Fig. 3. The bandstructures of A=Rb, K for $E_p = -0.2$ are shown in Fig. 11 in Appendix A. They are similar to that of A=Cs. $E_\Gamma \sim -0.6$ for A=Rb, K is also consistent with the ARPES measurements [49].

To perform the diagrammatic calculation, we introduce the 30×30 matrix expression of the Green function as

$$\hat{G}(k) = [(i\epsilon_n + \mu)\hat{1} - \hat{h}^0(\mathbf{k})]^{-1}, \quad (6)$$

where μ is the chemical potential.

Next, we calculate the effects of the strong Coulomb interaction of $3d$ -orbital electrons on V sites. In kagome metals, the FSs are mainly composed of two of the five d -orbitals of V atom: The “pure-type” FS is composed of three d_{XZ} (or b_{3g} rep.) orbitals on sublattices A, B, C, and the “mix-type” FS is composed of three d_{YZ} orbitals (or b_{2g} rep.). In the pure-type FS, the bandstructure around each vHS- S ($S=A, B, C$) is composed of the single sublattice S , which is known as the “sublattice interference”. In contrast, in the mix-type FS, each vHS- S is composed of two of three sublattices. Both the pure-type and mix-type bands are nearly independent, although they weakly hybridize each other.

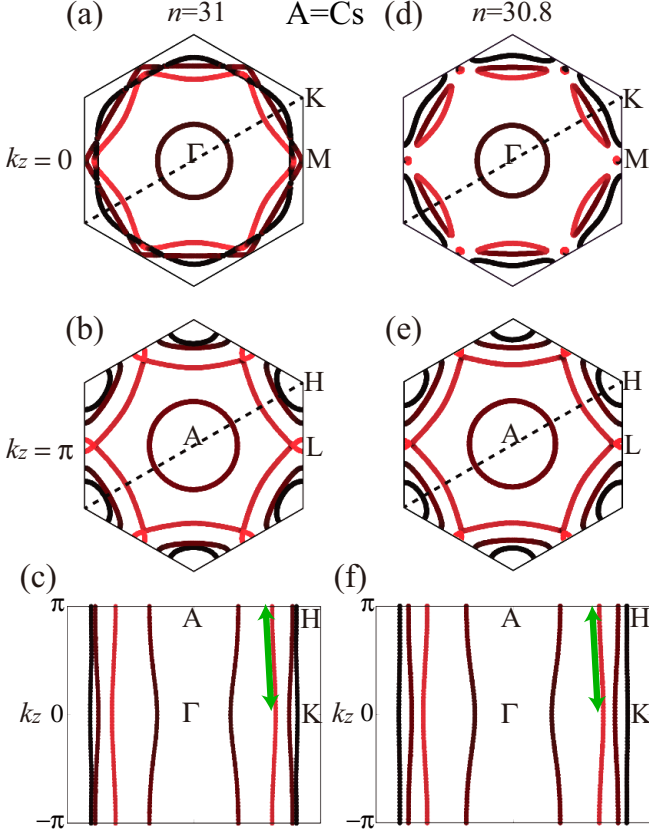


FIG. 3. FS structure of the present kagome metal model for $A=Cs$. The FS at $n = 31$ on the (a) $k_z = 0$ plane, (b) $k_z = \pi$ plane, and (c) plane including Γ KHA points along the dotted line in (a) and (b). The red color denotes the b_{3g} -orbital weight. The green arrow shows the nesting along the k_z direction. The FS at $n = 30.8$ on the (d) $k_z = 0$ plane, (e) $k_z = \pi$ plane, and (f) plane including Γ KHA points.

Here, we study the spin-channel and charge-channel susceptibilities, $\hat{\chi}^s(q)$ and $\hat{\chi}^c(q)$, based on the random-phase-approximation (RPA), which is equivalent to the

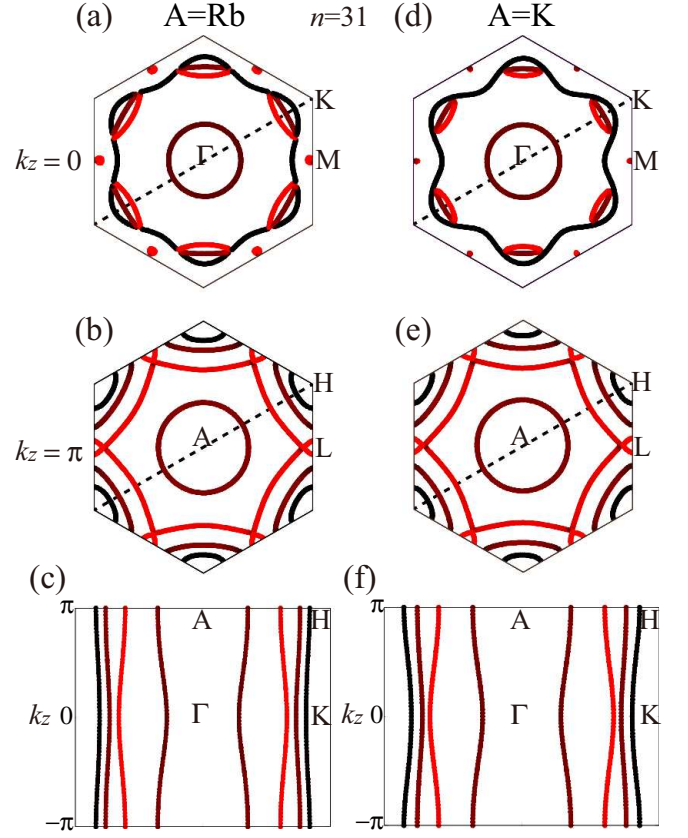


FIG. 4. FS structure of the present kagome metal models for $A=Rb, K$ at $n = 31$. The FS for $A=Rb$ on the (a) $k_z = 0$ plane, (b) $k_z = \pi$ plane, and (c) plane including Γ KHA points. The red color denotes the b_{3g} -orbital weight. The FS for $A=K$ on the (d) $k_z = 0$ plane, (e) $k_z = \pi$ plane, and (f) plane including Γ KHA points.

mend-field approximation. In the RPA, it is given as

$$\hat{\chi}^{s(c)}(Q) = \hat{\chi}^0(q) \left[\hat{1} - \hat{\Gamma}^{s(c)} \hat{\chi}^0(Q) \right]^{-1}, \quad (7)$$

$$\chi_{ll',mm'}^0(Q) = -\frac{T}{N} \sum_k G_{lm}(k+Q) G_{m'l'}(k), \quad (8)$$

where $Q \equiv (Q, \omega_l)$ with the bosonic Matsubara frequency $\omega_l = 2\pi Tl$, and $\chi_{ll',mm'}^0(Q)$ is the irreducible susceptibility. Here, $\Gamma_{ll'mm'}^{s(c)}$ is the 5-orbital Coulomb interaction for the same sublattice in the spin (charge) channel, composed of the intra-orbital U , inter-orbital U' , and the exchange term $J = (U - U')/2$. The expression of $\Gamma_{ll'mm'}^{s(c)}$ is presented in Ref. [70, 71]. Here, we introduce the spin (charge) Stoner factor $\alpha_{S(C)}$ given as the largest eigenvalue of $\hat{\Gamma}^{s(c)} \hat{\chi}^0(q)$. $\chi^{s(c)}$ diverges when $\alpha_{S(C)}$ reaches unity. In the RPA, α_S is always larger than α_C [70, 71] for $U > U'$, so the nonmagnetic BO in kagome metals cannot be explained unless large nearest-neighbor Coulomb interaction V ($V > 0.5U$) exists. However, the BO and the current order are naturally explained by considering the beyond-mean-field electron correlations described by

the VCs.

In previous theoretical studies [12], both the spin and BO fluctuations develop in pure-type and mix-type FSs. It was shown that the electron correlations are stronger on pure-type FS composed of d_{XZ} (or b_{3g}) orbitals. Therefore, in the present study, we consider the on-site Coulomb interactions only on the b_{3g} orbitals. Here, we assign $l = 1, 2, 3$ to the b_{3g} orbital on sites A, B, C, respectively. In this case, the Coulomb interaction is simply given as $\hat{\Gamma}_{mm',ll'}^{s(c)} = U^{s(c)}\delta_{m,m'}\delta_{l,l'}\delta_{l,m}$, where $U^s = U$ and $U^c = -U$. Then, the RPA susceptibility is simplified as

$$\hat{\chi}^{s(c)}(Q) = \hat{\chi}^0(Q) \left[\hat{1} - (+)U\hat{\chi}^0(Q) \right]^{-1}, \quad (9)$$

where $\hat{\chi}^{s(c)}(q)$ is 3×3 matrix: $\hat{\chi}_{l,m}^0(Q) = \chi_{ll,mm}^0(Q)$ with $l, m = 1, 2, 3$. In the next section, we introduce the DW equation to study the BO in kagome metals. The kernel function (with MT-term and AL-terms) of the DW equation is composed of the RPA susceptibility.

IV. DW EQUATION ANALYSIS FOR 3D KAGOME METAL MODEL

Here, we study the BO in the 3D kagome metal models based on the DW equation theory. In this theory, various nonmagnetic DW orders are caused by the beyond-RPA non-local correlations. This theory was first developed to explain the orbital nematic state in Fe-based superconductors, and it has been successfully applied to the cuprates [72] and the twisted-bilayer graphene [73]. Recently, the present authors studied 2D kagome metals in Ref. [12]. By solving the DW equation shown in Fig. 5 (a), we can calculate the infinite series of AL and MT terms. The AL terms represent the PMI mechanism, which gives rise to the BO in kagome metals. The analytic expression of the charge-channel DW equation is

$$\lambda_{\mathbf{Q}} g_{\mathbf{Q}}^L(k) = -\frac{T}{N} \sum_{p, M_1, M_2} I_{\mathbf{Q}}^{L, M_1}(k, p) \times \{G(p)G(p + \mathbf{Q})\}^{M_1, M_2} g_{\mathbf{Q}}^{M_2}(p), \quad (10)$$

where $k \equiv (\mathbf{k}, \epsilon_n)$ and $p \equiv (\mathbf{p}, \epsilon_m)$. The largest eigenvalue $\lambda_{\mathbf{Q}}$ represents the DW instability at wavevector \mathbf{Q} , and the corresponding form factor $\hat{g}_{\mathbf{Q}}$ gives the DW order function. $L \equiv (l, l')$ and M_i represent the pair of sublattice indices A, B, C . The phase factor of the eigenvector is fixed to satisfy the Hermitian condition $g_{\mathbf{Q}}^{ll'}(\mathbf{k}, \epsilon_n) = [g_{-\mathbf{Q}}^{l'l}(\mathbf{k} + \mathbf{Q}, -\epsilon_n)]^*$. In addition, we fix the sign of $\hat{g}_{\mathbf{Q}_m}$ so that $\phi_m \hat{g}_{\mathbf{Q}_m}$ reproduces the BO shown in Fig. 1.

The effective interaction $\hat{I}_{\mathbf{Q}}(k, p)$ in the DW equation is given as

$$I_{\mathbf{Q}}^{l'l', mm'}(k, k') = \sum_{b=s,c} \frac{a^b}{2} \left[-V_{lm, l'm'}^b(k - k') \right.$$

$$\left. + \frac{T}{N} \sum_p \sum_{l_1 l_2, m_1 m_2} V_{l_1, mm_1}^b(p + \mathbf{Q}) V_{m' m_2, l' l_2}^b(p) \times G_{l_1 l_2}(k - p) G_{m_2 m_1}(k' - p) \right. \\ \left. + \frac{T}{N} \sum_p \sum_{l_1 l_2, m_1 m_2} V_{l_1, m_2 m'}^b(p + \mathbf{Q}) V_{m_1 m, l' l_2}^b(p) \times G_{l_1 l_2}(k - p) G_{m_2 m_1}(k' + p + \mathbf{Q}) \right] \quad (11)$$

where $a^{s(c)} = 3(1)$ and $p = (\mathbf{p}, \omega_l)$. \hat{V}^b is the b -channel interaction given by $\hat{V}^b = \hat{\Gamma}^b + \hat{\Gamma}^b \hat{\chi}^b \hat{\Gamma}^b$.

Note that the form factor is proportional to the particle-hole condensation $\sum_{\sigma} \langle c_{\mathbf{k}+\mathbf{q}, l, \sigma}^{\dagger} c_{\mathbf{k}, l', \sigma} \rangle$, or equivalently, the symmetry-breaking component in the self-energy.

Here, we explain the obtained numerical results for A=Cs at $T = 0.04$ and $U = 2.6$, where $\alpha_S = 0.90$. Figure 5 (b) shows the obtained $\lambda_{\mathbf{Q}}$ on the $q^z = 0$ plane at $n = 30.8, 31$: $\lambda_{\mathbf{Q}}$ shows the almost commensurate peak at $\mathbf{q} = \mathbf{q}_1$, which corresponds to the 2D BO wavevector in kagome metals. Interestingly, the q_1^z -dependence of $\lambda_{\mathbf{Q}_1}$ is quite small ($\lesssim 1\%$), as shown in Fig. 5 (c), reflecting the 2D-character of the FSs in kagome metals. We note that the value of $\lambda_{\mathbf{Q}_1}$ for $q_1^z = \pi$ is slightly larger than that for $q_1^z = 0$ since the nesting vector with $k_z \sim \pi$ emerges in Figs. 3 (c) and (f), which derives the wavevector with $q^z \sim \pi$ as discussed in Ref. [30]. In this case, the alternating v-BO with $\{q_1^z, q_2^z, q_3^z\} = \{\pi, \pi, \pi\}$ is the most favorable, while the SoD (TrH) s-BO with $\{q_1^z, q_2^z, q_3^z\} = \{\pi, \pi, 0\}$ is also favored. Figures 5 (d) and (e) show α_S dependence of $\lambda_{\mathbf{Q}}$ for $q^z = 0$ at $n = 31$. $\lambda_{\mathbf{Q}_1}$ reaches 1 for $\alpha_S \gtrsim 0.97$. Thus, the BO transition temperature $T_{\text{BO}} \sim 100\text{K}$ is obtained in the moderate electron correlation.

In deriving Figs. 5 (b)-(e), we take only the Coulomb interaction on the b_{3g} orbital into account. This simplification does not alter the qualitative results, while the quantitative results are improved by considering the multiorbital Coulomb interaction.

Figure 6 shows \mathbf{Q} dependence of $\lambda_{\mathbf{Q}}$ for A=Rb, K at $T = 0.04$ with $\alpha_S = 0.90$, where $U = 2.5$ for A=Rb, K. The obtained results are similar to those for A=Cs shown in Fig. 5. Thus, it is robust that the alternating v-BO and the SoD (TrH) s-BO are favored in kagome metals.

To discuss the three dimensionality of the kagome metal model, we introduce the magnification factor r_z for the inter-layer hopping integrals. $r_z = 1$ corresponds to the original 3D kagome metal model, and $r_z = 0$ corresponds to the pure 2D model. Figure 7 (a) shows the obtained $\lambda_{(\mathbf{q}_1, \pi)}/\lambda_{(\mathbf{q}_1, 0)}$ as a function of r_z at $n = 31$ and $n = 30.8$ of A=Cs. In both cases, the obtained $\lambda_{(\mathbf{q}_1, \pi)}/\lambda_{(\mathbf{q}_1, 0)}$ exhibits a smooth r_z^2 behavior. Therefore, the obtained q^z -dependence of the eigenvalue due to the small inter-layer hopping integrals is considered to be accurately calculated. When the absolute value of r_z increases, the FS in $k_z = 0$ changes significantly while the FS in $k_z = \pi$ changes slightly. We find that the value of $\lambda_{(\mathbf{q}_1, \pi)}/\lambda_{(\mathbf{q}_1, 0)}$ peaks when the small FS composed of

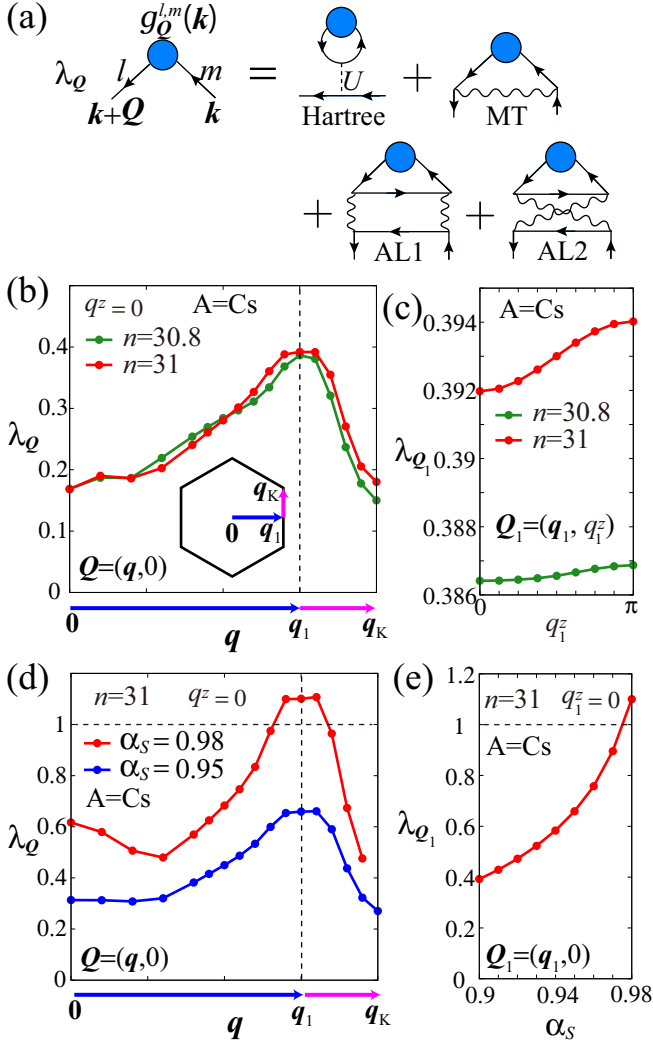


FIG. 5. (a) Charge-channel density-wave (DW) eigenvalue equation. The largest eigenvalue $\lambda_{\mathbf{Q}}$ represents the instability of the charge-channel DW at wavevector \mathbf{Q} , and the form factor f gives the order parameter. The wavy lines represent the spin susceptibilities. Two AL terms describe the paramagnon interference mechanism that gives various unconventional DW states. (b-c) Obtained $\lambda_{\mathbf{Q}}$ for A=Cs at $n = 30.8, 31$: (b) $\lambda_{\mathbf{Q}}$ in the $q^z = 0$ plane, where $\mathbf{q}_{\mathbf{K}} = \left(\frac{2\pi}{\sqrt{3}}, \frac{2\pi}{3}\right)$. (c) Small q_1^z -dependence of $\lambda_{\mathbf{Q}_1}$ for $\mathbf{Q}_1 = (q_1, q_1^z)$. The BO solution is obtained for any q_1^z . (d) $\lambda_{\mathbf{Q}}$ for $\alpha_S = 0.95, 0.98$ in $q^z = 0$ at $n = 31$ of A=Cs. (e) α_S dependence of $\lambda_{\mathbf{Q}_1}$ for $q_1^z = 0$ at $n = 31$ of A=Cs.

the b_{3g} orbital around L point disappears. The value of $\lambda_{(q_1, \pi)} / \lambda_{(q_1, 0)}$ is sensitive to the value of r_z , and it reaches 1.03 at $n = 31$ for $r_z = 2.25$, where the Q dependence of $\lambda_{\mathbf{Q}}$ is similar to that for $r_z = 1$, as shown in Figs. 5 (b) and 7 (b). In this case, the stability of the alternating v-BO with $\{q_1^z, q_2^z, q_3^z\} = \{\pi, \pi, \pi\}$ is strongly enhanced. We note that $r_z > 1$ is realized under pressure. Thus, pressure dependence may be explained by r_z dependence. In addition, the value of r_z would be effec-

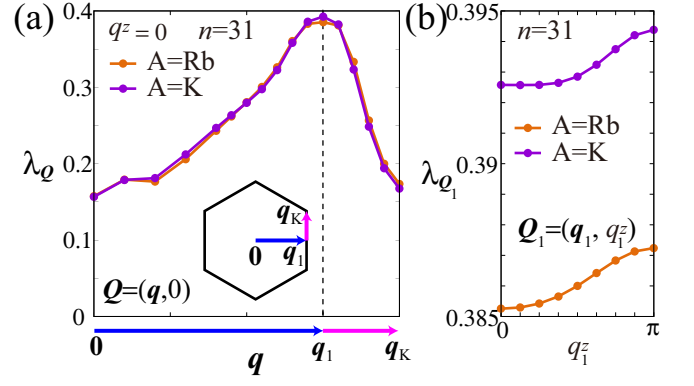


FIG. 6. (a-b) Obtained $\lambda_{\mathbf{Q}}$ for A=Rb, K at $n = 31$: (a) $\lambda_{\mathbf{Q}}$ in the $q^z = 0$ plane. (b) Small q_1^z -dependence of $\lambda_{\mathbf{Q}_1}$ for $\mathbf{Q}_1 = (q_1, q_1^z)$.

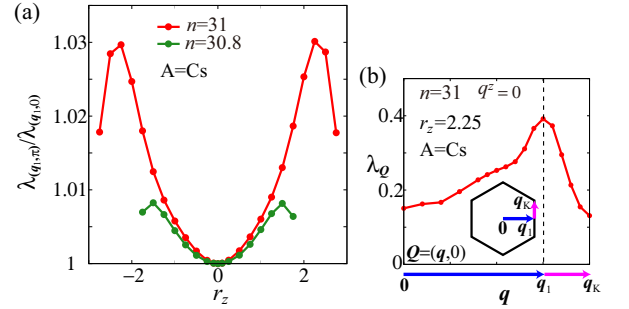


FIG. 7. (a) Obtained $\lambda_{(q_1, \pi)} / \lambda_{(q_1, 0)}$ as a function of r_z at $n = 31, 30.8$ of A=Cs. Here, r_z represents the magnification factor for the inter-layer hopping integrals. $r_z = 1$ corresponds to the original 3D kagome metal model of A=Cs. (b) $\lambda_{\mathbf{Q}}$ in the $q^z = 0$ plane for $r_z = 2.25$ at $n = 31$ of A=Cs.

tively enhanced by including the Coulomb interaction of b_{2g} orbitals, whose inter-layer hopping is about 10 times larger than b_{3g} orbitals. The q_z dependence of $\lambda_{\mathbf{Q}}$ in Fig. 5 would increase when the form factor includes the b_{2g} -orbital component.

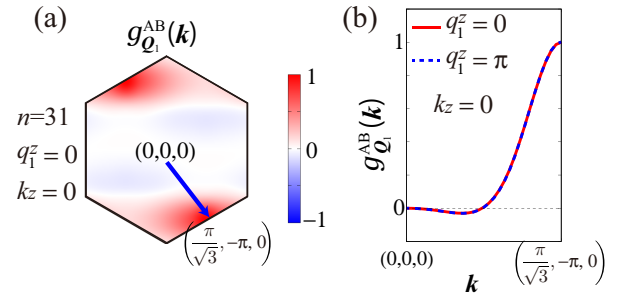


FIG. 8. (a) Obtained form factor $g_{\mathbf{Q}_1}^{\text{AB}}(\mathbf{k})$ in the k_x - k_y plane at $q_1^z = 0$ at $n = 31$ for $r_z = 1$. (b) \mathbf{k} dependence of $g_{\mathbf{Q}_1}^{\text{AB}}(\mathbf{k})$ for $q_1^z = 0, \pi$ along the blue arrow in (a).

Figure 8 (a) shows the obtained form factor $g_{\mathbf{Q}_1}^{\text{AB}}(\mathbf{k})$

in the k_x - k_y plane at $q_1^z = 0$ in the case of $n = 31$ and $r_z = 1$. Here, $\hat{g}_{\mathbf{Q}}(\mathbf{k}) \equiv \hat{g}_{\mathbf{Q}}(\mathbf{k}, 0)$ is given by the analytic continuation (linear extrapolation) of $\hat{g}_{\mathbf{Q}}(k)$. We also show the \mathbf{k} dependence of $g_{\mathbf{Q}_1}^{\text{AB}}(\mathbf{k})$ for $q_1^z = 0, \pi$ at $k_z = 0$ in Fig. 8 (b). q_1^z dependences of $g_{\mathbf{Q}_1}^{\text{AB}}(\mathbf{k})$ are quite small. We confirm that k_z dependences of $g_{\mathbf{Q}_1}^{\text{AB}}(\mathbf{k})$ is also negligible. Thus, we ignore the q^z and k_z dependences of the form factors.

To summarize, the eigenvalue for the BO $\lambda_{\mathbf{Q}}$ derived from the DW equation analysis for the 3D multiorbital kagome metal models for A=Cs, Rb, K shows the maximum value at commensurate $\mathbf{Q} = \mathbf{Q}_m$ ($m = 1, 2, 3$), while it is almost independent of q_m^z . This result would be consistent with the rich variety of the 3D BO states observed in kagome metals. In the present study, $\lambda_{(\mathbf{q}_m, \pi)}$ is slightly larger than $\lambda_{(\mathbf{q}_m, 0)}$. In this case, the alternating v-BO with $\{q_1^z, q_2^z, q_3^z\} = \{\pi, \pi, \pi\}$ in Fig. 2 (a) is the most favorable, while the SoD (TrH) s-BO with $\{q_1^z, q_2^z, q_3^z\} = \{\pi, \pi, 0\}$ in Fig. 2 (b) is also favored. These results are robust for all A=Cs, Rb, K models. However, competition between q^z -dependence of $\lambda_{(\mathbf{q}_m, q^z)}$ and that of the 3rd-order GL term would be important to discuss the 3D structure of CDW.

V. 3RD-ORDER GL COEFFICIENT

To understand the 3D 3Q BO state, we also study the 3rd-order GL term $b_1(q_1^z, q_2^z, q_3^z)$ in the 3D kagome metal models. Here, we fix the 2D BO wavevectors \mathbf{q}_m while their r_z components q_m^z are variables, under the constraint $q_1^z + q_2^z + q_3^z = 0$ (modulo 2π). Here, we take account of commensurate $q_m^z = -q_m^z (= 0, \pi)$ BO wavevectors. $b_1(q_1^z, q_2^z, q_3^z)$ is given as

$$\begin{aligned}
 b_1(q_1^z, q_2^z, q_3^z) = & -\frac{T}{N} \sum_{k, m_i} [g_{\mathbf{Q}_3}^{m_1 m_2}(\mathbf{k} + \mathbf{Q}_1 + \mathbf{Q}_2) \\
 & \times G_{m_2 m_3}(k + \mathbf{Q}_1 + \mathbf{Q}_2) g_{\mathbf{Q}_2}^{m_3 m_4}(\mathbf{k} + \mathbf{Q}_1) \\
 & \times G_{m_4 m_5}(k + \mathbf{Q}_1) g_{\mathbf{Q}_1}^{m_5 m_6}(\mathbf{k}) G_{m_6 m_1}(k) \\
 & + (\mathbf{Q}_2 \leftrightarrow \mathbf{Q}_3)], \quad (12)
 \end{aligned}$$

whose diagrammatic expression is given in Fig. 9 (a) [13]. Figure 9 (b) shows the numerical results for $r_z = 1$ and $r_z = 2$. In the case of the original model $r_z = 1$, the obtained negative b_1 favors the SoD (TrH) BO for $n \lesssim 31$ ($n > 31$). Since the obtained $b_1(\pi, \pi, 0)$ is almost the same as $b_1(0, 0, 0)$, $2 \times 2 \times 2$ SoD (TrH) BO competes with $2 \times 2 \times 1$ SoD (TrH) BO. In detail, $|b_1(\pi, \pi, 0)|$ is slightly larger than $|b_1(0, 0, 0)|$ for $n \lesssim 31$. In the case of $r_z = 2$, the obtained $|b_1(\pi, \pi, 0)|$ is larger than $|b_1(0, 0, 0)|$. Thus, the $\{q_1^z, q_2^z, q_3^z\} = \{\pi, \pi, 0\}$ nematic SoD s-BO is favored. This nematic BO is Z_3 nematic state, which is equivalent for $\{q_1^z, q_2^z, q_3^z\} = \{\pi, 0, \pi\}, \{0, \pi, \pi\}$. In general, the triangle diagram is sensitive to the nesting condition; see Fig. 1 in Ref. [72]. In the present 3D kagome metal models, 3D nesting with $q_z \sim \pi$ emerges as shown in Figs. 3 (c) and (f). We confirm that the q^z dependence

of the 4th-order GL coefficients is smaller than that of the 3rd-order one, as shown in Appendix B. Thus, the 3D structure of CDW would be determined by the q^z -dependence of $\lambda_{\mathbf{Q}}$ and b_1 . Therefore, the nematic shift stacking of the 3Q BOs discussed in Ref. [10, 64, 65] is a plausible candidate for the 3D BO state in kagome metals. Figure 9 (c) shows n dependence of $b_1(\pi, \pi, 0)$ and $b_1(0, 0, 0)$ for A=Rb, K. The result for A=Rb is similar to that for A=Cs, while the result for A=K corresponds to the hole-doped case for A=Cs. This result for A=K is consistent with the fact that the FSs of A=K are similar to those of the hole-doped Cs as shown in Figs 3 and 4. From these results, it is robust that $|b_1(\pi, \pi, 0)|$ is larger than $|b_1(0, 0, 0)|$ for $n \leq 31$. Thus, nematic SoD s-BO is favored by the 3rd-order GL term in all A=Cs, Rb, K kagome models.

In the NMR study for A=Cs [37, 56], the SoD BO has been proposed at low temperatures, while other NMR studies have proposed the TrH s-BO near the CDW transition temperature. The SoD BO at low temperatures is consistent with the 3rd-order GL analysis in the present study at $n = 31$. However, the TrH BO, which is realized for $b_1 > 0$, may compete with the SoD BO since the obtained value of $b_1 < 0$ is very small at $n = 31$ as shown in Figs. 9 (b) and (c). In addition, we note that these BOs are favored by the DW equation due to the PMI mechanism, where the most favorable 3D structure is the alternating v-BO. These competitions would explain the rich variety of the 3D DW states in kagome metals.

VI. DISCUSSION

Here, we discuss the 3D structure of CDW in kagome metal based on the obtained results by the 3D DW equation and the 3rd-order GL free energy. From the \mathbf{Q} dependence of $\lambda_{\mathbf{Q}}$ shown in Figs. 5 and 6, we find that $\lambda_{\mathbf{q}_1, \pi}$ slightly dominates over $\lambda_{\mathbf{q}_1, 0}$. In addition, the difference between $\lambda_{\mathbf{q}_1, \pi}$ and $\lambda_{\mathbf{q}_1, 0}$ increases with the magnification factor for the inter-layer hopping integrals r_z as shown in Fig. 7 (a). $r_z > 1$ would be realized by applying the pressure and considering the Coulomb interaction for b_{2g} orbitals. Thus, the commensurate $2 \times 2 \times 2$ alternating v-BO with $\{q_1^z, q_2^z, q_3^z\} = \{\pi, \pi, \pi\}$ is realized based on the 3D DW equation due to the PMI mechanism.

On the other hand, from the $\{q_1^z, q_2^z, q_3^z\}$ dependence of $b_1(q_1^z, q_2^z, q_3^z)$ shown in Fig. 9 (b), $|b_1(\pi, \pi, 0)|$ is slightly larger than $|b_1(0, 0, 0)|$ ($b_1 < 0$) for $n \lesssim 31$. The difference between $|b_1(\pi, \pi, 0)|$ and $|b_1(0, 0, 0)|$ also increases with r_z . Thus, the commensurate $2 \times 2 \times 2$ Z_3 nematic SoD s-BO for $\{q_1^z, q_2^z, q_3^z\} = \{\pi, \pi, 0\}, \{\pi, 0, \pi\}, \{0, \pi, \pi\}$ is favored by the 3rd-order GL free energy.

We expect that the $2 \times 2 \times 2$ Z_3 nematic SoD s-BO replaces alternating v-BO when q_z dependence of b_1 is enough. In fact, these $2 \times 2 \times 2$ BOs have been observed in many experiments. Since the magnitude and sign of the coefficient b_1 depend sensitively and strongly on the

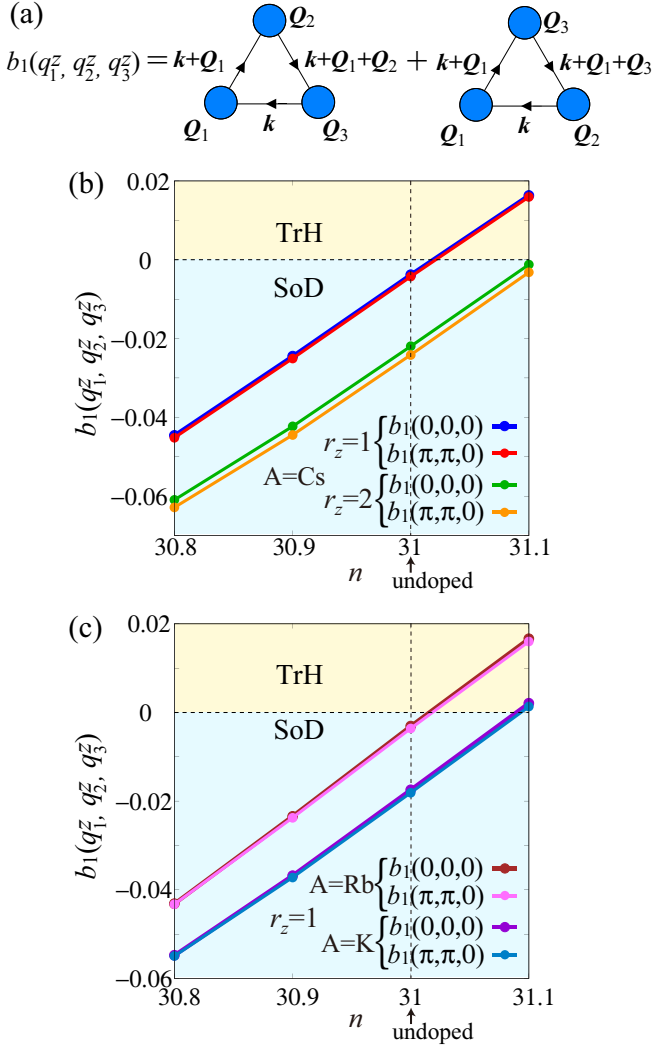


FIG. 9. (a) Diagrammatic expression of the 3rd-order GL coefficient $b_1(q_1^z, q_2^z, q_3^z)$. (b) $b_1(0, 0, 0)$ and $b_1(\pi, \pi, 0)$ as functions of n for $r_z = 1$ and $r_z = 2$ at $T = 0.08$ for $A=Cs$. Here, r_z represents the magnification factor for the inter-layer hopping integrals. (c) $b_1(0, 0, 0)$ and $b_1(\pi, \pi, 0)$ as functions of n for $r_z = 1$ at $T = 0.08$ for $A=Rb, K$.

band structure, the rich variety of BOs observed in experiments would be understood by the combination of the DW equation analysis and the 3rd-order GL free energy. We verify that the PMI mechanism in the DW equation is essential origin of the 3D CDW in kagome metals.

VII. SUMMARY

In summary, we studied the 3D nature of the DW in kagome metals based on the 3D multiorbital models for AV_3Sb_5 ($A=Cs, Rb, K$), by using the DW equation method in combination with the GL theory. The SoD or TrH shape commensurate BO is robustly induced in each V-Sb plane by the PMI mechanism that is described

by the AL-VCs. $T_{BO} \sim 100K$ is obtained in the moderate electron correlation. In the DW equation analysis for all $A=Cs, Rb, K$ models, we revealed that (i) the most favorable 3D structure is the alternating v-BO, and (ii) the Z_3 nematic SoD or TrH s-BO is also energetically favorable in the PMI mechanism. We found that these Z_3 nematic s-BO states can be realized by considering the small 3rd-order GL free energy. Since the 3rd-order GL free energy depends sensitively and strongly on the band structure, both (i) the v-BO and (ii) the s-BO states can be realized. The rich variety of BOs observed in experiments can be understood by the combination of the DW equation analysis and the 3rd-order GL free energy. It was confirmed that the PMI mechanism is the essential origin of the 3D CDW of kagome metals.

Appendix A: 3D Fermi surface and bandstructure

We derive the 30 orbital tight-binding model with 15 V d -orbitals and 15 Sb p -orbitals by using the WIEN2k [67] and Wannier90 [68] software. Figure 10 (a) shows the bandstructures for $\Delta E_p = -0.2, 0$. The bandstructure around the Γ point is composed of Sb p -orbitals. By introducing $\Delta E_p = -0.2$, energy at the Γ point E_Γ decreases from $-0.4eV$ to $-0.55eV$ consistently with ARPES measurements [49, 69]. Figure 10 (b) shows the 3D FS for $\Delta E_p = -0.2$ at $n = 31$. Figures 11 (a) and (b) show the bandstructures of $A=Rb$ and $A=K$ for $\Delta E_p = -0.2$, respectively. In these case, $E_\Gamma \sim -0.6$ is also consistent with ARPES measurements [49].

Appendix B: 3rd- and 4th-order GL coefficients in the presence of BOs and current orders

Here, we calculate the 3rd- and 4th-order GL coefficients based on the diagrammatic method. The GL free energy is given as

$$\begin{aligned}
 F^{(3)} &= b_1 \phi_1 \phi_2 \phi_3 + b_2 (\phi_1 \eta_2 \eta_3 + \eta_1 \phi_2 \eta_3 + \eta_1 \eta_2 \phi_3), \quad (B1) \\
 F^{(4)} &= d_{1,a} (\phi_1^4 + \phi_2^4 + \phi_3^4) + d_{1,b} (\phi_1^2 \phi_2^2 + \phi_2^2 \phi_3^2 + \phi_3^2 \phi_1^2) \\
 &\quad + d_{2,a} (\eta_1^4 + \eta_2^4 + \eta_3^4) + d_{2,b} (\eta_1^2 \eta_2^2 + \eta_2^2 \eta_3^2 + \eta_3^2 \eta_1^2) \\
 &\quad + 2d_{3,a} (\phi_1^2 \eta_1^2 + \phi_2^2 \eta_2^2 + \phi_3^2 \eta_3^2) \\
 &\quad + d_{3,b} (\phi_1^2 \eta_2^2 + \phi_2^2 \eta_3^2 + \phi_3^2 \eta_1^2 + \phi_2^2 \eta_1^2 + \phi_3^2 \eta_2^2 + \phi_1^2 \eta_3^2). \quad (B2)
 \end{aligned}$$

where form factors are normalized as $\max_{\mathbf{k}} |g_{Q_1}^{AB}(\mathbf{k})| = \max_{\mathbf{k}} |f_{Q_1}^{AB}(\mathbf{k})| = 1$ which is realized at $\mathbf{k} = \mathbf{k}_A$ in the present DW equation analysis. Then, the BO parameter $\phi_m \hat{g}_{Q_m}$ for $m = 1 \sim 3$ gives the hybridization gap $\Delta_{BO} \sim |\phi|$ in the folded band at Γ point. In the same way, $\Delta_{cLC} \sim |\eta|$ for the chiral charge current order $\eta_m \hat{f}_{Q_m}$. Thus, the present normalization rule for g and f is physically reasonable and convenient.

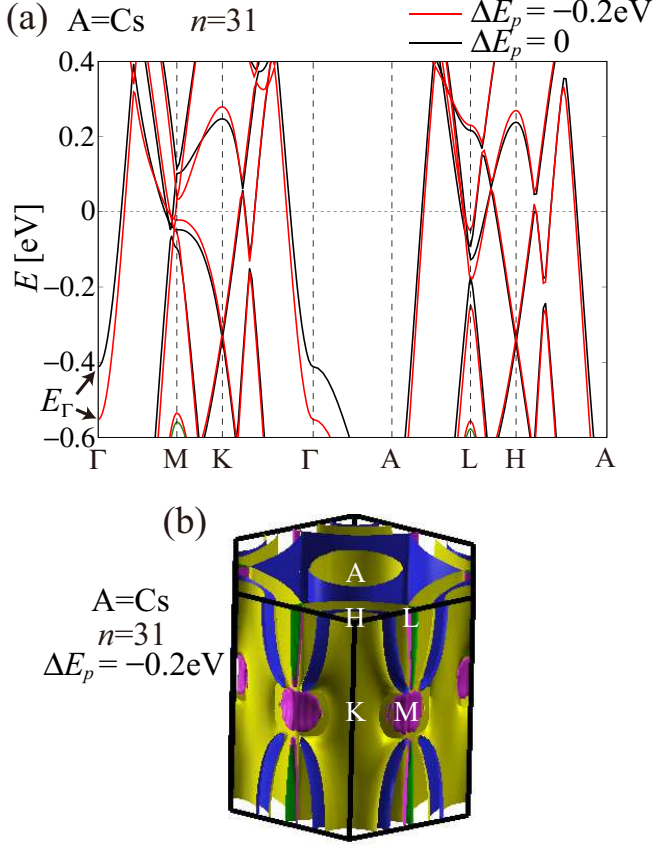


FIG. 10. (a) Bandstructure of A=Cs for $\Delta E_P = 0$ (black line) and that for $\Delta E_P = -0.2$ (red line). (b) Three-dimensional FSs of A=Cs for $\Delta E_P = -0.2$.

The 3rd-order GL parameters per unit cell are given as

$$b_1 = 3I_{123}^{ggg} + 3I_{132}^{ggg}, \quad (\text{B3})$$

$$b_2 = 3I_{123}^{gff} + 3I_{132}^{gff}, \quad (\text{B4})$$

where

$$I_{lmn}^{xyz} = -\frac{T}{3N} \sum_{k,\sigma} \text{Tr} \hat{x}_{\mathbf{Q}_l}(\mathbf{k} + \mathbf{Q}_n + \mathbf{Q}_m) \hat{G}(k + \mathbf{Q}_n + \mathbf{Q}_m) \\ \times \hat{y}_{\mathbf{Q}_m}(\mathbf{k} + \mathbf{Q}_n) \hat{G}(k + \mathbf{Q}_n) \hat{z}_{\mathbf{Q}_n}(\mathbf{k}) \hat{G}(k), \quad (\text{B5})$$

where $\hat{x}, \hat{y}, \hat{z}$ is \hat{f} or \hat{g} , and l, m, n is 1, 2, or 3. The relation $q_l + q_m + q_n = 0$ should be satisfied. Here, we take account of commensurate $q_m^z = -q_n^z (= 0, \pi)$ BO wavevectors.

Figure 12 (a) shows the diagrammatic expression of the 4th-order GL coefficient $d_{1,a}(q_1^z, q_1^z, q_1^z, q_1^z)$ given as

$$d_{1,a}(q_1^z, q_1^z, q_1^z, q_1^z) = \frac{T}{4N} \sum_{k, m_i} g_{\mathbf{Q}_1}^{m_1 m_2}(\mathbf{k} + \mathbf{Q}_1) G_{m_2 m_3}(k + \mathbf{Q}_1) \\ \times g_{\mathbf{Q}_1}^{m_3 m_4}(\mathbf{k}) G_{m_4 m_5}(k) \\ \times g_{\mathbf{Q}_1}^{m_5 m_6}(\mathbf{k} + \mathbf{Q}_1) G_{m_6 m_7}(k + \mathbf{Q}_1)$$

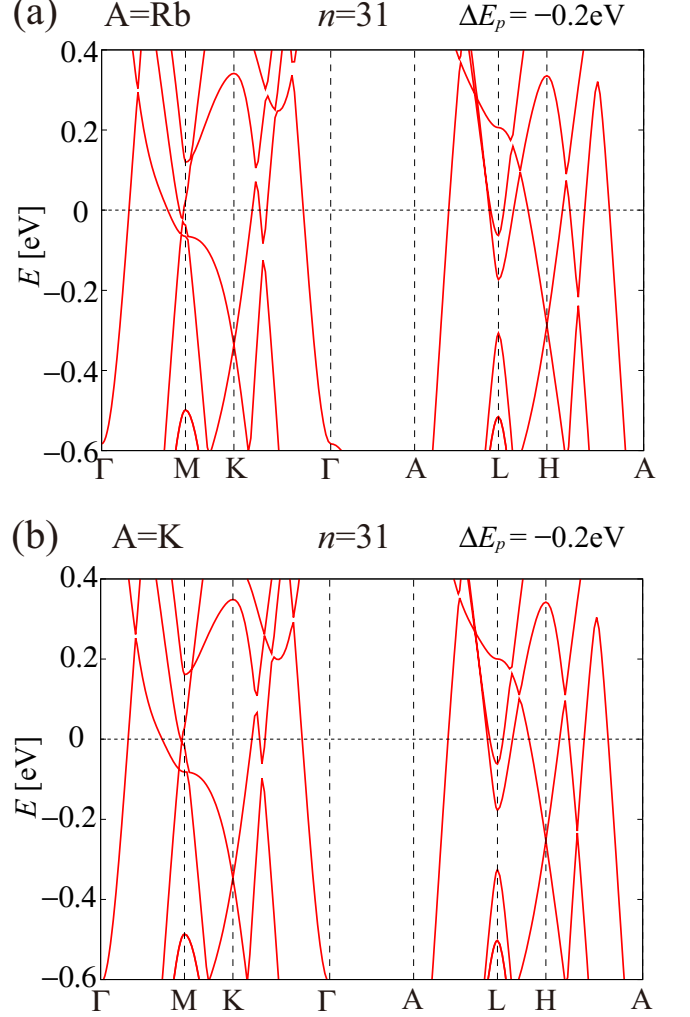


FIG. 11. (a) Bandstructure of A=Rb for $\Delta E_P = -0.2$ and (b) that of A=K.

$$\times g_{\mathbf{Q}_1}^{m_7 m_8}(\mathbf{k}) G_{m_8 m_1}(k), \quad (\text{B6})$$

We perform the numerical calculation of $d_{1,a}(q_1^z, q_1^z, q_1^z, q_1^z)$ in 3D kagome metal model with $\Delta E_P = -0.2$. Figure 12 (b) shows the obtained $d_{1,a}(q_1^z, q_1^z, q_1^z, q_1^z)$ at $q_1^z = 0, \pi$ for $r_z = 1$ and $r_z = 2$ for A=Cs. The obtained q^z -dependence of $d_{1,a}$ is smaller than that of the 2nd and 3rd-order GL coefficients. Thus, the 3D structure of CDW would be determined by the q^z -dependence of $\lambda_{\mathbf{Q}}$ and b_1 .

ACKNOWLEDGMENTS

This work was supported by JSPS KAKENHI Grants No. JP24K00568, No. JP24K06938, No. JP23K03299, and No. JP22K14003.

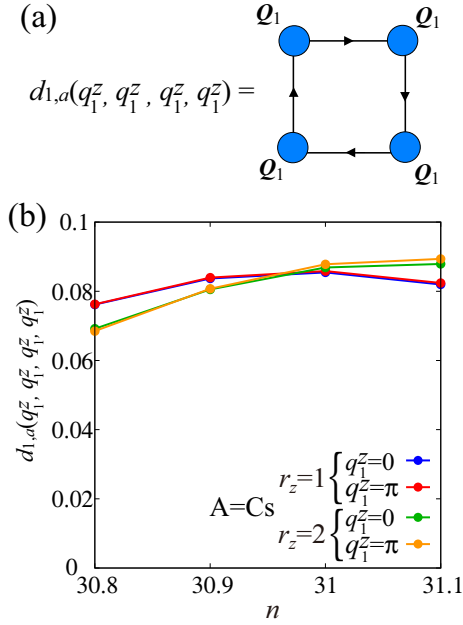


FIG. 12. (a) Diagrammatic expression of the 4th-order GL coefficient $d_{1,a}(q_1^z, q_1^z, q_1^z, q_1^z)$. (b) Obtained $d_{1,a}(q_1^z, q_1^z, q_1^z, q_1^z)$ as a function of n at $q_1^z = 0, \pi$ for $r_z = 1$ and $r_z = 2$ in the 3D kagome metal model with $\Delta E_p = -0.2$ at $T = 0.08$ for $A=Cs$.

-
- [1] B. R. Ortiz, L. C. Gomes, J. R. Morey, M. Winiarski, M. Bordelon, J. S. Mangum, I. W. H. Oswald, J. A. Rodriguez-Rivera, J. R. Neilson, S. D. Wilson, E. Ertekin, T. M. McQueen, and E. S. Toberer, *New kagome prototype materials: discovery of KV_3Sb_5 , RbV_3Sb_5 , and CsV_3Sb_5* , Phys. Rev. Materials **3**, 094407 (2019).
- [2] B. R. Ortiz, S. M. L. Teicher, Y. Hu, J. L. Zuo, P. M. Sarte, E. C. Schueller, A. M. M. Abeykoon, M. J. Krogstad, S. Rosenkranz, R. Osborn, R. Seshadri, L. Balents, J. He, and S. D. Wilson, *CsV_3Sb_5 : A \mathbb{Z}_2 Topological Kagome Metal with a Superconducting Ground State*, Phys. Rev. Lett. **125**, 247002 (2020).
- [3] F. H. Yu, D. H. Ma, W. Z. Zhuo, S. Q. Liu, X. K. Wen, B. Lei, J. J. Ying, and X. H. Chen, *Unusual competition of superconductivity and charge-density-wave state in a compressed topological kagome metal*, Nat. Commun. **12**, 3645 (2021).
- [4] Y.-X. Jiang, J.-X. Yin, M. M. Denner, N. Shumiya, B. R. Ortiz, G. Xu, Z. Guguchia, J. He, M. S. Hossain, X. Liu, J. Ruff, L. Kautzsch, S. S. Zhang, G. Chang, I. Belopolski, Q. Zhang, T. A. Cochran, D. Multer, M. Litskevich, Z.-J. Cheng, X. P. Yang, Z. Wang, R. Thomale, T. Neupert, S. D. Wilson, and M. Z. Hasan, *Unconventional chiral charge order in kagome superconductor KV_3Sb_5* , Nat. Mater. **20**, 1353 (2021).
- [5] H. Li, H. Zhao, B. R. Ortiz, T. Park, M. Ye, L. Balents, Z. Wang, S. D. Wilson, and I. Zeljkovic, *Rotation symmetry breaking in the normal state of a kagome superconductor KV_3Sb_5* , Nat. Phys. **18**, 265 (2022).
- [6] M. L. Kiesel, C. Platt, and R. Thomale, *Unconventional Fermi Surface Instabilities in the Kagome Hubbard Model*, Phys. Rev. Lett. **110**, 126405 (2013).
- [7] W.-S. Wang, Z.-Z. Li, Y.-Y. Xiang, and Q.-H. Wang, *Competing electronic orders on kagome lattices at van Hove filling*, Phys. Rev. B **87**, 115135 (2013).
- [8] X. Wu, T. Schwemmer, T. Müller, A. Consiglio, G. Sangiovanni, D. Di Sante, Y. Iqbal, W. Hanke, A. P. Schnyder, M. M. Denner, M. H. Fischer, T. Neupert, and R. Thomale, *Nature of Unconventional Pairing in the Kagome Superconductors AV_3Sb_5 ($A = K, Rb, Cs$)*, Phys. Rev. Lett. **127**, 177001 (2021).
- [9] M. M. Denner, R. Thomale, and T. Neupert, *Analysis of Charge Order in the Kagome Metal AV_3Sb_5 ($A = K, Rb, Cs$)*, Phys. Rev. Lett. **127**, 217601 (2021).
- [10] T. Park, M. Ye, and L. Balents, *Electronic instabilities of kagome metals: Saddle points and Landau theory*, Phys. Rev. B **104**, 035142 (2021).
- [11] Y.-P. Lin and R. M. Nandkishore, *Complex charge density waves at Van Hove singularity on hexagonal lattices: Haldane-model phase diagram and potential realization in the kagome metals AV_3Sb_5 ($A = K, Rb, Cs$)*, Phys. Rev. B **104**, 045122 (2021).
- [12] R. Tazai, Y. Yamakawa, S. Onari, and H. Kontani, *Mechanism of exotic density-wave and beyond-Migdal unconventional superconductivity in kagome metal AV_3Sb_5 ($A = K, Rb, Cs$)*, Sci. Adv. **8**, eabl4108 (2022).
- [13] R. Tazai, Y. Yamakawa, and H. Kontani, *Charge-loop current order and \mathbb{Z}_3 nematicity mediated by bond-order fluctuations in kagome metals*, Nat. Commun. **14**, 7845 (2023).

- (2023).
- [14] M. Roppongi, K. Ishihara, Y. Tanaka, K. Ogawa, K. Okada, S. Liu, K. Mukasa, Y. Mizukami, Y. Uwatoko, R. Grasset, M. Konczykowski, B. R. Ortiz, S. D. Wilson, K. Hashimoto, and T. Shibauchi, *Bulk evidence of anisotropic s-wave pairing with no sign change in the kagome superconductor CsV₃Sb₅*, Nat. Commun. **14**, 667 (2023).
- [15] W. Zhang, X. Liu, L. Wang, C. Wai T., Z. Wang, S. T. Lam, W. Wang, J. Xie, X. Zhou, Y. Zhao, S. Wang, J. Tallon, K. T. Lai, and S. K. Goh, *Nodeless superconductivity in kagome metal CsV₃Sb₅ with and without time reversal symmetry breaking*, Nano Lett., **23**, 872 (2023).
- [16] H. Tan, Y. Liu, Z. Wang, and B. Yan, *Charge Density Waves and Electronic Properties of Superconducting Kagome Metals*, Phys. Rev. Lett. **127**, 046401 (2021).
- [17] H. Li, T. T. Zhang, T. Yilmaz, Y. Y. Pai, C. E. Marvinney, A. Said, Q. W. Yin, C. S. Gong, Z. J. Tu, E. Vescovo, C. S. Nelson, R. G. Moore, S. Murakami, H. C. Lei, H. N. Lee, B. J. Lawrie, and H. Miao, *Observation of Unconventional Charge Density Wave without Acoustic Phonon Anomaly in Kagome Superconductors AV₃Sb₅ (A = Rb, Cs)*, Phys. Rev. X **11**, 031050 (2021).
- [18] H. Kontani, R. Tazai, Y. Yamakawa, and S. Onari, *Unconventional density waves and superconductivities in Fe-based superconductors and other strongly correlated electron systems*, Adv. Phys. **70**, 355 (2021).
- [19] C. Mielke, D. Das, J.-X. Yin, H. Liu, R. Gupta, Y.-X. Jiang, M. Medarde, X. Wu, H. C. Lei, J. Chang, P. Dai, Q. Si, H. Miao, R. Thomale, T. Neupert, Y. Shi, R. Khasanov, M. Z. Hasan, H. Luetkens, and Z. Guguchia, *Time-reversal symmetry-breaking charge order in a kagome superconductor*, Nature **602**, 245 (2022).
- [20] R. Khasanov, D. Das, R. Gupta, C. Mielke, M. Elender, Q. Yin, Z. Tu, C. Gong, H. Lei, E. T. Ritz, R. M. Fernandes, T. Birol, Z. Guguchia, and H. Luetkens, *Time-reversal symmetry broken by charge order in CsV₃Sb₅*, Phys. Rev. Research **4**, 023244 (2022).
- [21] Z. Guguchia, C. Mielke, D. Das, R. Gupta, J.-X. Yin, H. Liu, Q. Yin, M. H. Christensen, Z. Tu, C. Gong, N. Shumiya, M. S. Hossain, T. Gamsakhurdashvili, M. Elender, P. Dai, A. Amato, Y. Shi, H. C. Lei, R. M. Fernandes, M. Z. Hasan, H. Luetkens, and R. Khasanov, *Tunable unconventional kagome superconductivity in charge ordered RbV₃Sb₅ and KV₃Sb₅*, Nat. Commun. **14**, 153 (2023).
- [22] S.-Y. Yang, Y. Wang, B. R. Ortiz, D. Liu, J. Gayles, E. Derunova, R. Gonzalez-Hernandez, L. Šmejkal, Y. Chen, S. S. P. Parkin, S. D. Wilson, E. S. Toberer, T. McQueen, and M. N. Ali, *Giant, unconventional anomalous Hall effect in the metallic frustrated magnet candidate, KV₃Sb₅*, Sci. Adv. **6**, eabb6003 (2020).
- [23] F. H. Yu, T. Wu, Z. Y. Wang, B. Lei, W. Z. Zhuo, J. J. Ying, and X. H. Chen, *Concurrence of anomalous Hall effect and charge density wave in a superconducting topological kagome metal*, Phys. Rev. B **104**, L041103 (2021).
- [24] C. Guo, C. Putzke, S. Konyzheva, X. Huang, M. Gutierrez-Amigo, I. Errea, D. Chen, M. G. Vergniory, C. Felser, M. H. Fischer, T. Neupert, and P. J. W. Moll, *Switchable chiral transport in charge-ordered Kagome metal CsV₃Sb₅*, Nature **611**, 461 (2022).
- [25] C. Guo, G. Wagner, C. Putzke, D. Chen, K. Wang, L. Zhang, M. G. Amigo, I. Errea, M. G. Vergniory, C. Felser, M. H. Fischer, T. Neupert, and P. J. W. Moll, *Correlated order at the tipping point in the kagome metal CsV₃Sb₅*, Nat. Phys. **20**, 579 (2024).
- [26] T. Asaba, A. Onishi, Y. Kageyama, T. Kiyosue, K. Ohtsuka, S. Suetsugu, Y. Kohsaka, T. Gaggli, Y. Kasahara, H. Murayama, K. Hashimoto, R. Tazai, H. Kontani, B. R. Ortiz, S. D. Wilson, Q. Li, H. -H. Wen, T. Shibauchi, Y. Matsuda, *Evidence for an odd-parity nematic phase above the charge density wave transition in kagome metal CsV₃Sb₅*, Nat. Phys. **20**, 40 (2024).
- [27] M. H. Christensen, T. Biro, B. M. Andersen, and R. M. Fernandes, *Loop currents in AV₃Sb₅ kagome metals: Multipolar and toroidal magnetic orders*, Phys. Rev. B **106**, 144504 (2022).
- [28] H. D. Scammell, J. Ingham, T. Li, and O. P. Sushkov, *Chiral excitonic order from twofold van Hove singularities in kagome metals*, Nat. Commun. **14**, 605 (2023).
- [29] S. Onari, Y. Yamakawa, and H. Kontani, *Sign-Reversing Orbital Polarization in the Nematic Phase of FeSe due to the C₂ Symmetry Breaking in the Self-Energy*, Phys. Rev. Lett. **116**, 227001 (2016).
- [30] S. Onari and H. Kontani, *Hidden antiferromagnetic order in Fe-based superconductor BaFe₂As₂ and NaFeAs above T_S*, Phys. Rev. Research **2**, 042005(R) (2020).
- [31] S. Onari and H. Kontani, *Three-dimensional bond-order instability in infinite-layer nickelates due to nonlocal quantum interference*, Phys. Rev. B **108**, L241119 (2023).
- [32] *Electronic nature of charge density wave and electron-phonon coupling in kagome superconductor KV₃Sb₅*, Nat. Commun. **13**, 273 (2022).
- [33] Y.-X. Jiang, J.-X. Yin, M. M. Denner, N. Shumiya, B. R. Ortiz, G. Xu, Z. Guguchia, J. He, M. S. Hossain, X. Liu, J. Ruff, L. Kautzsch, S. S. Zhang, G. Chang, I. Belopolski, Q. Zhang, T. A. Cochran, D. Multer, M. Litskevich, Z.-J. Cheng, X. P. Yang, Z. Wang, R. Thomale, T. Neupert, S. D. Wilson, and M. Z. Hasan, *Unconventional chiral charge order in kagome superconductor KV₃Sb₅*, Nat. Mater. **20**, 1353 (2021).
- [34] Z. Wang, Y.-X. Jiang, J.-X. Yin, Y. Li, G.-Y. Wang, H.-L. Huang, S. Shao, J. Liu, P. Zhu, N. Shumiya, M. S. Hossain, H. Liu, Y. Shi, J. Duan, X. Li, G. Chang, P. Dai, Z. Ye, G. Xu, Y. Wang, H. Zheng, J. Jia, M. Z. Hasan, and Y. Yao, *Electronic nature of chiral charge order in the kagome superconductor CsV₃Sb₅*, Phys. Rev. B **104**, 075148 (2021).
- [35] L. Nie, K. Sun, W. Ma, D. Song, L. Zheng, Z. Liang, P. Wu, F. Yu, J. Li, M. Shan, D. Zhao, S. Li, B. Kang, Z. Wu, Y. Zhou, K. Liu, Z. Xiang, J. Ying, Z. Wang, T. Wu, and X. Chen, *Charge-density-wave-driven electronic nematicity in a kagome superconductor*, Nature **604**, 59 (2022).
- [36] T. Kato, Y. Li, T. Kawakami, M. Liu, K. Nakayama, Z. Wang, A. Moriya, K. Tanaka, T. Takahashi, Y. Yao, and T. Sato, *Three-dimensional energy gap and origin of charge-density wave in kagome superconductor KV₃Sb₅*, Commun. Mater. **3**, 30 (2022).
- [37] J. Luo, Z. Zhao, Y. Z. Zhou, J. Yang, A. F. Fang, H. T. Yang, H. J. Gao, R. Zhou, and G.-Q. Zheng, *Possible star-of-David pattern charge density wave with additional modulation in the kagome superconductor CsV₃Sb₅*, npj Quantum Mater. **7**, 30 (2022).
- [38] Z. Liu, N. Zhao, Q. Yin, C. Gong, Z. Tu, M. Li, W. Song, Z. Liu, D. Shen, Y. Huang, K. Liu, H. Lei, and S. Wang, *Charge-Density-Wave-Induced Bands Renormalization and Energy Gaps in a Kagome Superconductor RbV₃Sb₅*, Phys. Rev. X **11**, 041010 (2021).

- [39] S. Cho, H. Ma, W. Xia, Y. Yang, Z. Liu, Z. Huang, Z. Jiang, X. Lu, J. Liu, Z. Liu, J. Li, J. Wang, Y. Liu, J. Jia, Y. Guo, J. Liu, and D. Shen, *Emergence of New van Hove Singularities in the Charge Density Wave State of a Topological Kagome Metal RbV_3Sb_5* , Phys. Rev. Lett. **127**, 236401 (2021).
- [40] Y. Hu, X. Wu, B. R. Ortiz, X. Han, N. C. Plumb, S. D. Wilson, A. P. Schnyder, and M. Shi, *Coexistence of trihexagonal and star-of-David pattern in the charge density wave of the kagome superconductor AV_3Sb_5* , Phys. Rev. B **106**, L241106 (2022).
- [41] Q. Stahl, D. Chen, T. Ritschel, C. Shekhar, E. Sadrolahi, M. C. Rahn, O. Ivashko, M. v. Zimmermann, C. Felser, and J. Geck, *Temperature-driven reorganization of electronic order in CsV_3Sb_5* , Phys. Rev. B **105**, 195136 (2022).
- [42] Z. Liang, X. Hou, F. Zhang, W. Ma, P. Wu, Z. Zhang, F. Yu, J.-J. Ying, K. Jiang, L. Shan, Z. Wang, and X.-H. Chen, *Three-Dimensional Charge Density Wave and Surface-Dependent Vortex-Core States in a Kagome Superconductor CsV_3Sb_5* , Phys. Rev. X **11**, 031026 (2021).
- [43] Y. Wang, T. Wu, Z. Li, K. Jiang, and J. Hu, *Structure of the kagome superconductor CsV_3Sb_5 in the charge density wave state*, Phys. Rev. B **107**, 184106 (2023).
- [44] J. Frassinetti, P. Bonfá, G. Allodi, E. Garcia, R. Cong, B. R. Ortiz, S. D. Wilson, R. D. Renzi, V. F. Mitrović, and S. Sanna, *Microscopic nature of the charge-density wave in the kagome superconductor RbV_3Sb_5* , Phys. Rev. Research **5**, L012017 (2023).
- [45] C. Mu, Q. Yin, Z. Tu, C. Gong, P. Zheng, H. Lei, Z. Li, and J. Luo, *Tri-Hexagonal charge order in kagome metal CsV_3Sb_5 revealed by ^{121}Sb NQR*, Chin. Phys. B **31**, 017105 (2022).
- [46] D. W. Song, L. X. Zheng, F. H. Yu, J. Li, L. P. Nie, M. Shan, D. Zhao, S. J. Li, B. L. Kang, Z. M. Wu, Y. B. Zhou, K. L. Sun, K. Liu, X. G. Luo, Z. Y. Wang, J. J. Ying, X. G. Wan, T. Wu, and X. H. Chen, *Orbital ordering and fluctuations in a kagome superconductor CsV_3Sb_5* , Sci. China. Phys. Mech. Astron. **65**, 247462 (2022).
- [47] Z. Jiang, H. Ma, W. Xia, Z. Liu, Q. Xiao, Z. Liu, Y. Yang, J. Ding, Z. Huang, J. Liu, Y. Qiao, J. Liu, Y. Peng, S. Cho, Y. Guo, J. Liu, and D. Shen, *Observation of Electronic Nematicity Driven by the Three Dimensional Charge Density Wave in Kagome Lattice KV_3Sb_5* , Nano Lett. **23**, 5625 (2023).
- [48] H. Li, T. T. Zhang, T. Yilmaz, Y. Y. Pai, C. E. Marvinney, A. Said, Q. W. Yin, C. S. Gong, Z. J. Tu, E. Vescovo, C. S. Nelson, R. G. Moore, S. Murakami, H. C. Lei, H. N. Lee, B. J. Lawrie, and H. Miao, *Observation of Unconventional Charge Density Wave without Acoustic Phonon Anomaly in Kagome Superconductors AV_3Sb_5 ($A=Rb, Cs$)*, Phys. Rev. X **11**, 031050 (2021).
- [49] M. Kang, S. Fang, J. Yoo, B. R. Ortiz, Y. M. Oey, J. Choi, S. H. Ryu, J. Kim, C. Jozwiak, A. Bostwick, E. Rotenberg, E. Kaxiras, J. G. Checkelsky, S. D. Wilson, J.-H. Park, and R. Comin, *Charge order landscape and competition with superconductivity in kagome metals*, Nat. Mater. **22**, 186 (2023).
- [50] H. Li, G. Fabbris, A. H. Said, J. P. Sun, Y.-X. Jiang, J.-X. Yin, Y.-Y. Pai, S. Yoon, A. R. Lupini, C. S. Nelson, Q. W. Yin, C. S. Gong, Z. J. Tu, H. C. Lei, J.-G. Cheng, M. Z. Hasan, Z. Wang, B. Yan, R. Thomale, H. N. Lee, and H. Miao, *Discovery of conjoined charge density waves in the kagome superconductor CsV_3Sb_5* , Nat. Commun. **13**, 6348 (2022).
- [51] L. Kautzsch, B. R. Ortiz, K. Mallayya, J. Plumb, G. Pokharel, J. P. C. Ruff, Z. Islam, E.-A. Kim, R. Seshadri, S. D. Wilson, *Structural evolution of the kagome superconductors AV_3Sb_5 ($A = K, Rb, \text{ and } Cs$) through charge density wave order*, Phys. Rev. Materials **7**, 024806 (2023).
- [52] Q. Xiao, Y. Lin, Q. Li, X. Zheng, S. Francoual, C. Plueckthun, W. Xia, Q. Qiu, S. Zhang, Y. Guo, J. Feng, and Y. Peng, *Coexistence of multiple stacking charge density waves in kagome superconductor CsV_3Sb_5* , Phys. Rev. Research **5**, L012032 (2023).
- [53] J. Plumb, A. C. Salinas, K. Mallayya, E. Kisiel, F. B. Carneiro, R. Gomez, G. Pokharel, E.-A. Kim, S. Sarker, Z. Islam, S. Daly, S. D. Wilson, *Phase-Separated Charge Order and Twinning Across Length Scales in CsV_3Sb_5* , arXiv:2408.08842.
- [54] B. R. Ortiz, S. M. L. Teicher, L. Kautzsch, P. M. Sarte, N. Ratchiff, J. Harter, J. P. C. Ruff, R. Seshadri, and S. D. Wilson, *Fermi Surface Mapping and the Nature of Charge-Density-Wave Order in the Kagome Superconductor CsV_3Sb_5* , Phys. Rev. X **11**, 041030 (2021).
- [55] S. Wu, B. R. Ortiz, H. Tan, S. D. Wilson, B. Yan, T. Birol, and G. Blumberg, *Charge density wave order in the kagome metal AV_3Sb_5 ($A=Cs, Rb, K$)*, Phys. Rev. B **105**, 155106 (2022).
- [56] X. Y. Feng, Z. Zhao, J. Luo, J. Yang, A. F. Fang, H. T. Yang, H. J. Gao, R. Zhou, and G.-Q. Zheng, *Commensurate-to-incommensurate transition of charge-density-wave order and a possible quantum critical point in pressurized kagome metal CsV_3Sb_5* , npj Quantum Mater. **8**, 23 (2023).
- [57] H. Tan, Y. Liu, Z. Wang, and B. Yan, *Charge Density Waves and Electronic Properties of Superconducting Kagome Metals*, Phys. Rev. Lett. **127**, 046401 (2021).
- [58] Andrzej Ptok, Aksel Kobialka, Malgorzata Sternik, Jan Łażewski, Pawel T. Jochym, Andrzej M. Oleś, and Przemyslaw Piekarczyk, *Dynamical study of the origin of the charge density wave in AV_3Sb_5 ($A=K, Rb, Cs$) compounds*, Phys. Rev. B **105**, 235134 (2022).
- [59] C. Wang, S. Liu, H. Jeon, Y. Jia, and J.-H. Cho, *Charge density wave and superconductivity in the kagome metal CsV_3Sb_5 around a pressure-induced quantum critical point*, Phys. Rev. Materials **6**, 094801 (2022).
- [60] C. Wang, S. Liu, H. Jeon, and J.-H. Cho, *Origin of charge density wave in the layered kagome metal CsV_3Sb_5* , Phys. Rev. B **105**, 045135 (2022).
- [61] H. Li, X. Liu, Y. B. Kim, and H.-Y. Kee, *Origin of π -shifted three-dimensional charge density waves in the kagome metal AV_3Sb_5 ($A=Cs, Rb, K$)*, Phys. Rev. B **108**, 075102 (2023).
- [62] F. Grandi, A. Consiglio, M. A. Sentef, R. Thomale, and D. M. Kennes, *Theory of nematic charge orders in kagome metals*, Phys. Rev. B **107**, 155131 (2023).
- [63] F. Ferrari, F. Becca, and R. Valentí, *Charge density waves in kagome-lattice extended Hubbard models at the van Hove filling*, Phys. Rev. B **106**, L081107 (2022).
- [64] M. H. Christensen, T. Birol, B. M. Andersen, and R. M. Fernandes, *Theory of the charge density wave in AV_3Sb_5 kagome metals*, Phys. Rev. B **104**, 214513 (2021).
- [65] E. T. Ritz, R. M. Fernandes, and T. Birol, *Impact of Sb degrees of freedom on the charge density wave phase diagram of the kagome metal CsV_3Sb_5* , Phys. Rev. B **107**,

- 205131 (2023).
- [66] R. Tazai, S. Matsubara, Y. Yamakawa, S. Onari, and H. Kontani, *A Rigorous Formalism of Unconventional Symmetry Breaking in Fermi Liquid Theory and Its Application to Nematicity in FeSe*, Phys. Rev. B **107**, 035137 (2023).
- [67] P. Blaha, K. Schwarz, F. Tran, R. Laskowski, G. K. H. Madsen, and L. D. Marks, *WIEN 2K : An APW+lo Program for Calculating the Properties of Solids*, J. Chem. Phys. **152**, 074101 (2020).
- [68] G. Pizzi *et al.*, *Wannier90 as a community code: new features and applications*, J. Phys. Cond. Matt. **32**, 165902 (2020).
- [69] Y. Hu, X. Wu, B. R. Ortiz, S. Ju, X. Han, J. Ma, N. C. Plumb, M. Radovic, R. Thomale, S. D. Wilson, A. P. Schnyder, and M. Shi, *Rich nature of Van Hove singularities in Kagome superconductor CsV₃Sb₅*, Nat. Commun. **13**, 2220 (2022).
- [70] H. Kontani and S. Onari, *Orbital-Fluctuation-Mediated Superconductivity in Iron Pnictides: Analysis of the Five-Orbital Hubbard-Holstein Model*, Phys. Rev. Lett. **104**, 157001 (2010).
- [71] S. Onari and H. Kontani, *Self-consistent Vertex Correction Analysis for Iron-based Superconductors: Mechanism of Coulomb Interaction-Driven Orbital Fluctuations*, Phys. Rev. Lett. **109**, 137001 (2012).
- [72] Y. Yamakawa and H. Kontani, *Spin-Fluctuation-Driven Nematic Charge-Density Wave in Cuprate Superconductors: Impact of Aslamazov-Larkin Vertex Corrections*, Phys. Rev. Lett. **114**, 257001 (2015).
- [73] S. Onari and H. Kontani, *SU(4) Valley + Spin Fluctuation Interference Mechanism for Nematic Order in Magic-Angle Twisted Bilayer Graphene: The Impact of Vertex Corrections*, Phys. Rev. Lett. **128**, 066401 (2022).